EUROPEAN ORGANISATION FOR NUCLEAR RESEARCH

CERN-PPE/92-118
13 July 1992

A Measurement of Strange Baryon Production in Hadronic Z^0 Decays

OPAL Collaboration

Abstract

The production of the octet and decuplet baryons Λ, Ξ^-, $\Sigma(1385)^{\pm}$, $\Xi(1530)^0$ and Ω^- and the corresponding antibaryons has been measured in a sample of 485,000 hadronic Z^0 decays. Results on differential and integrated cross sections are presented. The differential cross section of Λ baryons is found to be softer than the one predicted by the Jetset and Herwig Monte Carlo generators. The measured decuplet yields are found to disagree with the simple diquark picture where only one tuning parameter for spin 1 diquarks is used. Comparisons of the momentum spectra for Λ and Ξ^- with the predictions of an analytical QCD formula are also presented.

Submitted to Physics Letters B

The OPAL Collaboration

P.D. Acton[25], G. Alexander[23], J. Allison[16], P.P. Allport[5], K.J. Anderson[9], S. Arcelli[2], A. Astbury[28], D. Axen[29], G. Azuelos[18,a], G.A. Bahan[16], J.T.M. Baines[16], A.H. Ball[17], J. Banks[16], R.J. Barlow[16], S. Barnett[16], J.R. Batley[5], G. Beaudoin[18], A. Beck[23], J. Becker[10], T. Behnke[27], K.W. Bell[20], G. Bella[23], P. Berlich[10], S. Bethke[11], O. Biebel[3], U. Binder[10], I.J. Bloodworth[1], P. Bock[11], B. Boden[3], H.M. Bosch[11], S. Bougerolle[29], H. Breuker[8], R.M. Brown[20], A. Buijs[8], H.J. Burckhart[8], P. Capiluppi[2], R.K. Carnegie[6], A.A. Carter[13], J.R. Carter[5], C.Y. Chang[17], D.G. Charlton[8], P.E.L. Clarke[25], I. Cohen[23], J.C. Clayton1, W.J. Collins[5], J.E. Conboy[15], M. Cooper[22], M. Coupland[14], M. Cuffiani[2], S. Dado[22], G.M. Dallavalle[2], S. De Jong[8], L.A. del Pozo[5], H. Deng[17], A. Dieckmann[11], M. Dittmar[4], M.S. Dixit[7], E. do Couto e Silva[12], J.E. Duboscq[8], E. Duchovni[26], G. Duckeck[11], I.P. Duerdoth[16], D.J.P. Dumas[6], P.A. Elcombe[5], P.G. Estabrooks[6], E. Etzion[23], H.G. Evans[9], F. Fabbri[2], M. Fincke-Keeler[28], H.M. Fischer[3], D.G. Fong[17], M. Foucher[17], A. Gaidot[21], O. Ganel[26], J.W. Gary[4], J. Gascon[18], R.F. McGowan[16], N.I. Geddes[20], C. Geich-Gimbel[3], S.W. Gensler[9], F.X. Gentit[21], G. Giacomelli[2], V. Gibson[5], W.R. Gibson[13], J.D. Gillies[20], J. Goldberg[22], M.J. Goodrick[5], W. Gorn[4], C. Grandi[2], F.C. Grant[5], J. Hagemann[27], G.G. Hanson[12], M. Hansroul[8], C.K. Hargrove[7], P.F. Harrison[13], J. Hart[8], P.M. Hattersley[1], M. Hauschild[8], C.M. Hawkes[8], E. Heflin[4], R.J. Hemingway[6], R.D. Heuer[8], J.C. Hill[5], S.J. Hillier[1], T. Hilse[10], D.A. Hinshaw[18], J.D. Hobbs[8], P.R. Hobson[25], D. Hochman[26], R.J. Homer[1], A.K. Honma[28,a], C.P. Howarth[15], R.E. Hughes-Jones[16], R. Humbert[10], P. Igo-Kemenes[11], H. Ihssen[11], D.C. Imrie[25], A.C. Janissen[6], A. Jawahery[17], P.W. Jeffreys[20], H. Jeremie[18], M. Jimack[2], M. Jobes[1], R.W.L. Jones[13], P. Jovanovic[1], C. Jui[4], D. Karlen[6], K. Kawagoe[24], T. Kawamoto[24], R.K. Keeler[28], R.G. Kellogg[17], B.W. Kennedy[15], S. Kluth[5], T. Kobayashi[24], T.P. Kokott[3], S. Komamiya[24], L. Köpke[8], J.F. Kral[8], R. Kowalewski[6], J. von Krogh[11], J. Kroll[9], M. Kuwano[24], P. Kyberd[13], G.D. Lafferty[16], F. Lamarche[18], J.G. Layter[4], P. Le Du[21], P. Leblanc[18], A.M. Lee[17], M.H. Lehto[15], D. Lellouch[26], P. Lennert[11], C. Leroy[18], J. Letts[4], S. Levegrün[3], L. Levinson[26], S.L. Lloyd[13], F.K. Loebinger[16], J.M. Lorah[17], B. Lorazo[18], M.J. Losty[7], X.C. Lou[12], J. Ludwig[10], M. Mannelli[8], S. Marcellini[2], G. Maringer[3], C. Markus[3], A.J. Martin[13], J.P. Martin[18], T. Mashimo[24], P. Mättig[3], U. Maur[3], J. McKenna[28], T.J. McMahon[1], J.R. McNutt[25], F. Meijers[8], D. Menszner[11], F.S. Merritt[9], H. Mes[7], A. Michelini[8], R.P. Middleton[20], G. Mikenberg[26], J. Mildenberger[6], D.J. Miller[15], R. Mir[12], W. Mohr[10], C. Moisan[18], A. Montanari[2], T. Mori[24], M. Morii[24], T. Mouthuy[12,b], B. Nellen[3], H.H. Nguyen[9], M. Nozaki[24], S.W. O'Neale[8,c], F.G. Oakham[7], F. Odorici[2], H.O. Ogren[12], C.J. Oram[28,a], M.J. Oreglia[9], S. Orito[24], J.P. Pansart[21], B. Panzer-Steindel[8], P. Paschievici[26], G.N. Patrick[20], N. Paz-Jaoshvili[23], P. Pfister[10], J.E. Pilcher[9], D. Pitman[28], D.E. Plane[8], P. Poffenberger[28], B. Poli[2], A. Pouladdej[6], E. Prebys[8], T.W. Pritchard[13], H. Przysiezniak[18], G. Quast[27], M.W. Redmond[9], D.L. Rees[1], G.E. Richards[16], D. Robinson[8], A. Rollnik[3], J.M. Roney[9], E. Ros[8], S. Rossberg[10], A.M. Rossi[2,d], M. Rosvick[28], P. Routenburg[6], K. Runge[10], O. Runolfsson[8], D.R. Rust[12], M. Sasaki[24], C. Sbarra[8], A.D. Schaile[10], O. Schaile[10], W. Schappert[6], P. Scharff-Hansen[8], P. Schenk[28], H. von der Schmitt[11], S. Schreiber[3], C. Schwick[27], J. Schwiening[3], W.G. Scott[20], M. Settles[12], T.G. Shears[5], B.C. Shen[4], C.H. Shepherd-Themistocleous[7], P. Sherwood[15], R. Shypit[29], A. Simon[3], P. Singh[13], G.P. Siroli[2], A. Skuja[17], A.M. Smith[8], T.J. Smith[8], G.A. Snow[17], R. Sobie[28,e], R.W. Springer[17], M. Sproston[20], K. Stephens[16], J. Steuerer[28], R. Ströhmer[11], D. Strom[30], T. Takeshita[24,f], P. Taras[18], S. Tarem[26], M. Tecchio[9], P. Teixeira-Dias[11], N. Tesch[3], N.J. Thackray[1], G. Transtromer[25], N.J. Tresilian[16], T. Tsukamoto[24], M.F. Turner[5], G. Tysarczyk-Niemeyer[11],

D. Van den plas[18], R. Van Kooten[8], G.J. VanDalen[4], G. Vasseur[21], C.J. Virtue[7], A. Wagner[27], D.L. Wagner[9], C. Wahl[10], J.P. Walker[1], C.P. Ward[5], D.R. Ward[5], P.M. Watkins[1], A.T. Watson[1], N.K. Watson[8], M. Weber[11], P. Weber[6], S. Weisz[8], P.S. Wells[8], N. Wermes[11], M.A. Whalley[1], G.W. Wilson[4], J.A. Wilson[1], V-H. Winterer[10], T. Wlodek[26], S. Wotton[11], T.R. Wyatt[16], R. Yaari[26], A. Yeaman[13], G. Yekutieli[26], M. Yurko[18], W. Zeuner[8], G.T. Zorn[17].

[1]School of Physics and Space Research, University of Birmingham, Birmingham, B15 2TT, UK
[2]Dipartimento di Fisica dell' Università di Bologna and INFN, Bologna, 40126, Italy
[3]Physikalisches Institut, Universität Bonn, D-5300 Bonn 1, FRG
[4]Department of Physics, University of California, Riverside, CA 92521 USA
[5]Cavendish Laboratory, Cambridge, CB3 0HE, UK
[6]Carleton University, Dept of Physics, Colonel By Drive, Ottawa, Ontario K1S 5B6, Canada
[7]Centre for Research in Particle Physics, Carleton University, Ottawa, Ontario K1S 5B6, Canada
[8]CERN, European Organisation for Particle Physics, 1211 Geneva 23, Switzerland
[9]Enrico Fermi Institute and Department of Physics, University of Chicago, Chicago Illinois 60637, USA
[10]Fakultät für Physik, Albert Ludwigs Universität, D-7800 Freiburg, FRG
[11]Physikalisches Institut, Universität Heidelberg, Heidelberg, FRG
[12]Indiana University, Dept of Physics, Swain Hall West 117, Bloomington, Indiana 47405, USA
[13]Queen Mary and Westfield College, University of London, London, E1 4NS, UK
[14]Birkbeck College, London, WC1E 7HV, UK
[15]University College London, London, WC1E 6BT, UK
[16]Department of Physics, Schuster Laboratory, The University, Manchester, M13 9PL, UK
[17]Department of Physics and Astronomy, University of Maryland, College Park, Maryland 20742, USA
[18]Laboratoire de Physique Nucléaire, Université de Montréal, Montréal, Quebec, H3C 3J7, Canada
[20]Rutherford Appleton Laboratory, Chilton, Didcot, Oxfordshire, OX11 0QX, UK
[21]DPhPE, CEN Saclay, F-91191 Gif-sur-Yvette, France
[22]Department of Physics, Technion-Israel Institute of Technology, Haifa 32000, Israel
[23]Department of Physics and Astronomy, Tel Aviv University, Tel Aviv 69978, Israel
[24]International Centre for Elementary Particle Physics and Dept of Physics, University of Tokyo, Tokyo 113, and Kobe University, Kobe 657, Japan
[25]Brunel University, Uxbridge, Middlesex, UB8 3PH UK
[26]Nuclear Physics Department, Weizmann Institute of Science, Rehovot, 76100, Israel
[27]Universität Hamburg/DESY, II Inst für Experimental Physik, 2000 Hamburg 52, Germany
[28]University of Victoria, Dept of Physics, P O Box 3055, Victoria BC V8W 3P6, Canada
[29]University of British Columbia, Dept of Physics, 6224 Agriculture Road, Vancouver BC V6T 1Z1, Canada
[30]University of Oregon, Dept of Physics, Eugene, Oregon 97403, USA

[a]Also at TRIUMF, Vancouver, Canada V6T 2A3
[b]Now at Centre de Physique des Particules de Marseille, Faculté des Sciences de Luminy, Marseille
[c]On leave from Birmingham University, Birmingham B15 2TT, UK
[d]Now at Dipartimento di Fisica, Università della Calabria and INFN, 87036 Rende, Italy
[e]And IPP, McGill University, High Energy Physics Department, 3600 University Str, Montreal, Quebec H3A 2T8, Canada
[f]Also at Shinshu University, Matsumoto 390, Japan

1 Introduction

Previous experiments at PETRA and PEP have measured the production of various baryon[1] species in jets [1]. It has been found that the average hadronic event at centre of mass energies of 29 GeV contains 0.58 $\pm$ 0.05 protons, 0.214 $\pm$ 0.012 Λ's, 0.035 $\pm$ 0.009 $\Sigma(1385)^{\pm}$'s and 0.0178 $\pm$ 0.0036 Ξ^-'s [2]. Surprisingly high rates for the Ω^- of 0.014 $\pm$ 0.007 have been reported [3]. The differential momentum spectra of mesons and baryons are found to be very similar, and consequently it is assumed that baryons and mesons are produced by a similar mechanism during the fragmentation process. However, the observed production ratio of Ξ^- to Λ and the small rates of decuplet baryons require additional mechanisms to suppress the production of baryons with single and double strangeness and with spin 3/2.

The observed momentum spectra and the extra suppression factors can be described by the diquark model, the most common approach used to describe baryon production in jets. According to this scheme, quark-antiquark and diquark-antidiquark pairs are produced from the sea. A diquark combines with a quark to form a baryon. This model, as used for example within the Lund String Model [4], leads naturally to similar fragmentation functions for baryons and light mesons. Thus far, these diquark models are in agreement with the observed baryon yields, if the free parameters to produce diquarks with different spin and strangeness are tuned appropriately.

Inclusive measurements of Λ and Ξ^- baryons have been published, based on about 90,000 hadronic Z^0 decays [5]. In this letter, the production of Λ, Ξ^-, $\Sigma(1385)^{\pm}$, $\Xi(1530)^0$, and Ω^- is measured with the OPAL detector using a sample of 485,000 hadronic Z^0 decays. These particles are identified via their decays over essentially the entire momentum range and allow a measurement of the differential and integrated yields with very good accuracy.

After a brief description of the OPAL detector and the selection of hadronic Z^0 decays, we describe the criteria used to select the different types of baryons. The cross sections are presented and compared with the Jetset Monte Carlo model version 7.3 [4] and with predictions of an analytical QCD formula. Production yields of strange baryons within the Herwig Monte Carlo version 5.0 [6] are also discussed.

2 The OPAL detector and the hadronic event selection

The crucial components for this analysis are described briefly below. A detailed description of the OPAL detector can be found elsewhere [7].

The measurements of the trajectories and momenta of charged particles are performed with a precision vertex chamber, a jet chamber and z-chambers. The cylindrical vertex drift chamber is located between radii of 9 and 24 cm and is subdivided into 36 azimuthal sectors each with 12 anode wires parallel to the beam direction and 36 sectors each with 6 anode wires at an average stereo angle of 4.1 degrees.

[1] To simplify the text, we use "baryons" to mean "baryons plus antibaryons", if not specified otherwise.

In the r-ϕ plane[2], the average space resolution is 50 μm for the hit nearest to the anode wire (first hit) and 90 μm for subsequent hits. The jet chamber is a large volume drift chamber, 4 m long and 1.85 m in radius, which is divided into 24 azimuthal sectors. Each sector contains a sense-wire plane having 159 axial anode wires. Each of the wires provides three-dimensional coordinate measurements, via drift-time measurement in the r-ϕ plane and charge-division measurement in the z direction. The average space point resolution in the r-ϕ plane is 130 μm. The jet chamber also allows the measurement of the specific energy loss, $\mathrm{d}E/\mathrm{d}x$, of charged particles [8]. A resolution of 3-4% has been obtained allowing particle identification over a large momentum range. In the barrel region ($|\cos\theta|$ less than 0.72), the jet chamber is surrounded by a set of z-chambers covering 94% of the azimuth, each of which has 6 anode wires perpendicular to the beam direction. This provides z coordinate measurements with an accuracy of approximately 300 μm. For larger $|\cos\theta|$ values, the last measured hit on a track can be used to measure θ with good accuracy. The three drift chamber detectors are operated at a gas pressure of 4 bar and are placed inside a solenoidal coil that provides a uniform axial magnetic field of 0.435 T.

Tracks are reconstructed using a method that explicitly incorporates the effect of multiple coulomb scattering in the detector gaseous volumes, in the discrete material between chambers, and in the beam pipe [9]. The momentum resolution in the r-ϕ plane for charged particles in the region $|\cos\theta| < 0.7$ is $(\sigma(p_t)/p_t)^2 = 0.02^2 + (0.0018 \cdot p_t)^2$, where p_t is the momentum in the r-ϕ plane in GeV. The impact parameter resolution in the r-ϕ plane, measured using $\mathrm{Z}^0 \to \mu^+\mu^-$ and $\mathrm{Z}^0 \to \mathrm{e}^+\mathrm{e}^-$ decays, is 40 μm for 45 GeV tracks. This resolution degrades to $\approx$ 65 μm at 10 GeV transverse momentum and to almost 300 μm at 1 GeV due to multiple scattering effects. Angular resolutions have been estimated to be approximately 0.1 mrad in ϕ and 2 mrad in θ for tracks measured in all components of the central detector.

The data sample, which corresponds to an integrated luminosity of about 20 pb^{-1}, was collected with the OPAL detector at LEP during 1990 and 1991. With the requirement that the three drift chambers are operational, a sample of 485,000 hadronic Z^0 decays has been selected using the criteria described in the OPAL line-shape analysis [10], with an efficiency of 98.4$\pm$0.4%. The remaining background processes are estimated to be at a negligible level (0.1% or less).

To determine the selection efficiencies for the different baryons, we have used a sample of approximately 400,000 Jetset hadronic Z^0 decays which have been passed through the full detector simulation program of the OPAL experiment [11]. In the case of the Ω^-, which has a very low cross section within the Jetset Monte Carlo, we have generated a special sample of 1300 hadronic events containing at least one Ω^- which decays to $\Lambda\mathrm{K}^-$, to determine the efficiency with better accuracy.

[2]The coordinate system is defined such that the z axis follows the electron beam direction, and the x axis is pointing in the direction of the centre of the LEP ring. The radial coordinate, r, is in the $x-y$ plane. The polar and azimuthal angles, θ and ϕ, are defined with respect to the z and x axes, respectively.

3 Selection of the different strange baryons

The Λ, Ξ^- and Ω^- can be identified by their decays into $p\pi^-$ (64%), $\Lambda\pi^-$ (100%) and ΛK^- (67.8%), respectively, with the corresponding branching ratios given in parentheses. Due to the long lifetimes of these baryons, a very strong rejection of combinatorial background is achieved by selecting particle combinations with secondary vertices, which are clearly displaced from the main vertex. In addition, the good dE/dx measurement in the jet chamber allows a further strong background suppression. For the identification of Ξ^- and Ω^-, the wrong charge combination provides an excellent method to determine the remaining background.

The $\Sigma(1385)^{\pm}$ and $\Xi(1530)^0$ decay strongly with branching ratios of 88% to $\Lambda\pi^{\pm}$ and 67% to $\Xi^-\pi^+$, respectively. Because of the prompt decay, no additional secondary vertex cuts are possible to reduce the combinatorial background.

For the measurements described below we require that:

- tracks have at least 40 associated wire hits (N_{hit}) of the jet chamber,
- the first reconstructed hit is before a radial distance of 140 cm,
- more than 50% of the geometrically possible hits are found, and
- the transverse momentum of the track with respect to the beam axis (p_t) is at least 100 MeV.

3.1 Λ selection

Two similar selection methods are used to select Λ's. The first method is optimized to obtain a very good mass resolution and a small systematic error. Here, both tracks used to identify the Λ decay must have associated z-chamber measurements. The polar angle θ is therefore limited to $|\cos\theta| < 0.7$. This method is used to derive the Λ cross section results.

The second method is optimized for high efficiency. This is achieved mainly because no requirements on the z-chambers are made, which extends the range of the polar angle to $|\cos\theta| < 0.9$, resulting in a slightly worse mass resolution for the additional identified Λ's. These reconstructed Λ's are used to identify the other baryon species.

Λ selection method 1

The following criteria are used for method 1:

- all track combinations with opposite charge are examined and the higher momentum track is assigned to be the proton track,
- the momentum of the combination must be above 1% of the beam energy,

- the impact parameter transverse to the beam direction (d_0) of the pion with respect to the main vertex[3] must be larger than 3 mm and the d_0 of the proton track must be larger than 1 mm,

- background is suppressed by using the information from the $\mathrm{d}E/\mathrm{d}x$ measurement, if available. Because of the cross-over regions [8], momentum dependent cuts are used. If more than 20 hits could be used for the $\mathrm{d}E/\mathrm{d}x$ measurement of a track, the combination is retained only if criterion 1 for the proton and criterion 2 for the pion are fulfilled:

  1. the higher momentum track has to have
     - a $\mathrm{d}E/\mathrm{d}x$ loss of more than 8 keV/cm and the probability[4] for a proton greater than 0.5% if the momentum is less than 1.5 GeV,
     - a $\mathrm{d}E/\mathrm{d}x$ loss of less than 8.5 keV/cm if the momentum is between 1.5 GeV and 2 GeV, where protons and pions both have a specific energy loss of about 7 keV/cm and
     - a probability for a proton of more than 5%, or alternatively the probability for a proton must be larger than the probability for a charged kaon, if the track momenta is above 2 GeV;
  2. for the lower momentum track the probability for a pion must be larger than 0.1%,

- photon conversions are removed if the invariant mass of the track pair, assuming them to be an electron positron pair, is smaller than 40 MeV,

- the selected combinations are required to have at least one track pair intersection within the radial range of $1 - 130$ cm on the side of the intersection point to which the combined momentum vector points. If two intersections exist, the one closer to the interaction point is normally used. The second solution is used (a) if both tracks have their first reconstructed hit after the second intersection point or (b) if one track has hits before and the other track has the first hit after the second intersection, and the angle in the plane transverse to the beam direction, Φ, between the direction of flight from the event vertex to the assumed decay point and the reconstructed Λ momentum, is smaller than for the first intersection.

- Candidates with hits on both tracks more than 5 cm upstream towards the collision point from the track intersection are removed, and

- the angle Φ must be smaller than 35 mrad.

With these cuts, a narrow, almost Gaussian Λ mass peak above a small background is obtained as shown in figure 1a. The mass obtained from a Gaussian fit to the peak, 1.1155 GeV $\pm$ 0.06 MeV, is in excellent agreement with the Particle Data Group value of 1.1156 GeV [2]. The resolution of the Λ mass is found to depend on momentum with a value of $\sigma = 2.3$ MeV for momenta below 5 GeV.

[3]The main vertex is fitted for each event using the measured track coordinates in the event.

[4]The difference between the measured and expected $\mathrm{d}E/\mathrm{d}x$ loss for a given particle type, assuming a Gaussian distribution with a known sigma, defines the probability.

The combinatorial background is determined for different momentum intervals by a fit to the mass distribution (x) using a Gaussian distribution for the Λ signal and a background of the form $(1.-e^{-a(x-1.077)}) \times (bx+c)$. The fit has been performed within a mass interval between 1.09 GeV and 1.20 GeV. Because of non-Gaussian tails, the number of Λ's is counted within an interval of $\pm$ 12 MeV around the Λ mass using the background estimated from the fit. Using this approach, a total of 17,384 Λ's above a background of 7,457 is found. The observed number of Λ's and the calculated background are given in table 1. We have used the same method in Monte Carlo generated events and find that this gives the correct number of Λ's with an accuracy of better than 3%. Using other background parametrisations and fit intervals, the obtained numbers also agree to better than 3%.

The different distributions of the geometrical variables used to select Λ's have been compared and very good agreement between data and Monte Carlo is found. The efficiency loss because of the requirement that both tracks have associated z-chamber hits is determined from the data. This efficiency for tracks within the geometrical acceptance of the z-chambers depends on the p_t of the tracks. At a p_t of 500 MeV, the efficiency is approximately 81%, and a maximum of 85% is reached for p_t above 2 GeV. The z-chamber efficiency in the data is found to be slightly lower than in the Monte Carlo. We find a value of the z-chamber efficiency of 96.5% relative to the Monte Carlo, essentially independent of p_t. The efficiency of method 1, including all corrections, is shown in figure 1c.

Several sources of systematic errors have been studied and are listed in table 1. After adding all errors in quadrature, the overall systematic error is found to be 5.6% for the Λ yield per hadronic event. The dominant errors are the uncertainty of the background estimation and of the cut simulation (4%).

The relative systematic error on the measured slope in the differential cross section is estimated, using Monte Carlo events, to be less than 5% over a 10 GeV Λ momentum interval.

Λ selection method 2

The following additional or slightly different selection criteria are used for method 2:

- no z-chamber requirements are made and the range of the polar angle is restricted to $|\cos\theta| < 0.9$ for Λ's,
- the impact parameter ($\hat{d_0}$) of the higher momentum track, assumed to be a proton, must be larger than 0.5 mm,
- in addition to the track pair intersection cuts described above, a momentum dependent cut on the decay distance is used. It is required that the probability of the Λ to have decayed before the calculated radial distance ($e^{-(m_\Lambda/p_t)\cdot(r/c\tau)}$, where $c\tau$ is the decay length, r the radial distance, and the other quantities are measured in GeV), be less than 95%. In addition, for small Λ momenta ($p_t < 1$ GeV), we require that this probability be greater than 2% (this cut excludes Λ's with very long decay distances),
- if the reconstructed radius of the decay point is smaller than 25 cm, it is required that the beam intersection point is found between the points of closest approach of the two tracks,

- the cut on the Φ angle (see above) of the Λ candidate is required to be smaller than 30 mrad and also smaller than 10 mrad + 20 mrad/$p_t(\Lambda)$, where $p_t(\Lambda)$ is measured in GeV, and
- the angle θ^* between the proton direction in the Λ rest frame and the Λ direction must satisfy $|\cos\theta^*| < 0.98$.

The resulting invariant mass distribution is shown in figure 1b. The number of Λ's is estimated within a signal region of $\pm$ 10 MeV for $x_E(\equiv E_\Lambda/E_{beam})$ smaller than 0.2 and $\pm$ 15 MeV for larger x_E values. The background is estimated by sideband subtraction, using the mass intervals between 1090-1100 MeV and 1130-1140 MeV. In the Monte Carlo events, we find that this method underestimates the background in the signal region by 20% for $x_E < 0.1$ and by 10% for larger momenta. The background estimated from the sidebands is therefore increased by this additional factor and subtracted from the events in the signal region. A systematic error of 50% is assigned for this correction factor. Thus a total of 30,041 Λ's above a background of 16,016 are reconstructed.

As a cross-check, a cross section is extracted for method 2. Different classes of Λ topology within the central detector are distinguished. As explained previously, the best mass resolution is obtained when both tracks have z-chamber coordinates. A slightly worse resolution with larger non-Gaussian tails is obtained for the other classes, where none of the tracks or either one of the two tracks has associated z-chamber information, or the ones with $|\cos\theta| > 0.72$, outside of the z-chamber acceptance.

The measured resolution increases almost linearly with momentum and is larger, between approximately $1.0 - 1.5$ MeV, in the data than in the Monte Carlo for each of the different classes, resulting in an extra loss in efficiency because more events are found outside the signal region. This extra loss in efficiency has been studied with the Monte Carlo and is found to be proportional to the resolution, reducing the efficiency of finding Λ's further by a factor of 0.925 ± 0.040 relative to the Monte Carlo. The efficiency is further corrected by the different z-chamber efficiencies in the data and the Monte Carlo. The efficiency of method 2, including all additional corrections mentioned above, is shown in figure 1c.

The different systematic errors are listed in table 1 and an overall systematic error of 8% is found for this method. The differential cross sections have been calculated separately for the different classes and are found to agree well with each other to within the estimated relative systematic errors up to an x_E of about 0.4. For higher momenta, reliable cross sections can only be obtained if both tracks have associated z-chamber hits. The corrected rates of this method also agree well with the ones obtained from method 1.

Λ candidates, selected with method 2, within the mass interval given above, are used to identify Ξ^-, $\Sigma(1385)^\pm$, Ω^- and $\Xi(1530)^0$, as described below.

3.2 Ξ^- selection

Ξ^- are identified by their decays into $\Lambda\pi^-$. Secondary vertices are selected using the following criteria:

- the d_0 of the additional pion track must be larger than 0.15 mm,
- an intersection of the track and the Λ must be found in the r-ϕ plane within a radial range of $1 - 50$ cm,
- the Φ angle of the $\Lambda\pi$ combination must be smaller than 30 mrad and also smaller than 10 mrad + 20 mrad/$p_t(\Xi)$, and
- if there are more than 20 hits available for the $\mathrm{d}E/\mathrm{d}x$ measurement, the combination is rejected if the probability of the additional track for a pion is smaller than 5% and the probability for an electron or a proton is larger than 5%.

With these cuts a narrow Ξ^- mass peak is observed as shown in figure 2a. Within an interval of ± 10 MeV around the nominal Ξ^- mass of 1.3213 GeV, we find 726 ± 38 events above a background of 388 events, determined from the wrong charge combination ($\Lambda\pi^+$). Dividing this sample into baryons and antibaryons we find 361 ± 27 Ξ^- and 365 ± 27 $\bar{\Xi}^+$ [5].

The efficiency obtained from the Monte Carlo is reduced by a factor of 0.91 ± 0.05 due to the slightly larger Λ mass resolution and different z-chamber efficiency in the data and is shown in figure 2b as a function of the Ξ^- energy. The different systematic uncertainties which have been studied are listed in table 1 and an overall systematic error of 9% is deduced.

3.3 Ω^- selection

Ω^- particles are identified via their decays into $\Lambda\mathrm{K}^-$ with secondary vertices. Due to larger background, stronger criteria are used relative to the ones in section 3.2:

- the kaon track candidate must have a p_t above 200 MeV and a d_0 larger than 0.15 mm,
- the Φ angle of the $\Lambda\mathrm{K}^-$ combination must be smaller than 30 mrad and also smaller than 10 mrad + 20 mrad/$p_t(\Omega^-)$,
- the charged kaon candidate must have more than 20 hits which are used for the $\mathrm{d}E/\mathrm{d}x$ measurement. If the momentum is smaller than 0.9 GeV, the kaon probability must be larger than 5% and the $\mathrm{d}E/\mathrm{d}x$ loss must be larger than 7.5 keV/cm. If the momentum is larger than 1.5 GeV, the probability to be a kaon must be larger than 5% and has also to be larger than the corresponding pion probability. In the cross-over region between 0.9 and 1.5 GeV, where identification of the kaon becomes difficult, the candidate is rejected.
- The probability of the calculated radial decay point of the $\Lambda\mathrm{K}^-$ combination, using the Ω^- lifetime ($e^{-(m_\Omega/p_t)\cdot(r/c\tau)}$), must be between 5% and 95%.

With these cuts the mass spectrum of figure 3a is obtained. A signal of 47 ± 11 events is found in an interval of ± 15 MeV around the Ω^- mass of 1.6724 GeV. The background of 42 events,

[5] Previous experiments at lower energies have all reported a slight excess of Ξ^- over $\bar{\Xi}^+$ with a combined significance of 3-4 standard deviations. This excess is not evident when our results are included.

shown as the histogram in figure 3a, is obtained from two sources. The dominant background is estimated from the wrong charge combination (ΛK^+). In addition, Ξ^- decays with misidentified pions contribute to the background in the correct charge combination. A total of 41 Ξ^- is found from the $\Lambda\pi$ mass peak. The invariant ΛK mass of these events does not show a peak in the Ω^- mass region and is separately shown as the shaded histogram.

Although the small statistics of the signal does not allow a detailed study of the systematics, several distributions in the data are found to be well described by the Monte Carlo. A large efficiency uncertainty of 13% comes from the small Monte Carlo statistics, leading to a total error of 17%, see table 1. This error should be compared to the statistical error of 24%.

3.4 $\Sigma(1385)^{\pm}$ and $\Xi(1530)^0$ selection

$\Sigma(1385)^{\pm}$ and $\Xi(1530)^0$ are identified via their prompt decays into $\Lambda\pi^{\pm}$ and $\Xi^-\pi^+$, respectively. The following criteria are used to combine the previously identified Λ and Ξ^- candidates with an additional charged particle:

- the d_0 of the track must be smaller than 2 mm, and
- if there are more than 20 hits useful for the $\mathrm{d}E/\mathrm{d}x$ measurement, the combination is rejected if the probability for a pion is smaller than 5% while the probability for an electron or a proton is larger than 5%.

With these cuts, a broad $\Sigma(1385)^{\pm}$ and a narrow $\Xi(1530)^0$ signal are clearly seen in figures 3b and 3c, respectively. In addition to the $\Sigma(1385)^{\pm}$ signal, a shoulder from Ξ^- decays is also seen in figure 3b.

The background for the $\Sigma(1385)^{\pm}$ has been determined using three different methods: (a) the shape from the Monte Carlo simulation, (b) fake Λ's from track pairs found outside the Λ mass region, and (c) fitting the $\Lambda\pi^{\pm}$ mass spectrum with a background function $(e^{-a(x-1.25)}) \times (bx^2 + cx)$, where x is the mass, a Breit-Wigner resonance with mass and width fixed to the $\Sigma(1385)^{\pm}$ mass and a Gaussian peak for the remaining Ξ^-. This fit is shown in figure 3b. The three different methods give the same result for the number of $\Sigma(1385)^{\pm}$'s to within 10%. The number of $\Sigma(1385)^{\pm}$'s from the fit is 2480 ± 250. The different contributions to the systematic error are listed in table 1, resulting in a total systematic error of 13%.

The background for the $\Xi(1530)^0$ is obtained using wrong charge $\Lambda\pi^+$ combinations, with masses between $1.29 - 1.35$ GeV. The Ξ^- mass is assigned to the wrong charge combinations, which are combined with additional oppositely charged tracks. The resulting mass distribution is shown as the histogram in figure 3c. After background subtraction, we estimate a total of 79 ± 13 $\Xi(1530)^0$ above a background of 83. A total systematic error of 16% is found from the different systematic uncertainties of this measurement as listed in table 1.

4 Cross section results and comparison with QCD predictions

The differential cross sections $(1/N_{had})dn/dx_E$ for $\Lambda, \Xi^-, \Sigma(1385)^{\pm}$ and $\Xi(1530)^0$ are given in tables 2, 3 and 4. The values of $(1/N_{had})dn/d\ln(1/x_p)$, with $x_p \equiv p/E_{beam}$, are given for Λ and Ξ^- in tables 2 and 3.

The differential cross sections $(1/N_{had})dn/dx_E$ are shown in figure 4a together with the Jetset Monte Carlo values normalised to the measured yield per hadronic event. The Λ momentum spectrum is softer than the corresponding one from Jetset: the data are roughly 20% lower for x_E above 0.2. The momentum spectrum of Λ's in the Herwig Monte Carlo is very similar to the Jetset one.

QCD calculations based on the modified leading log approximation (MLLA) [12] predict the shape of the ξ distribution ($\xi \equiv \ln(1/x_p)$) for soft gluons, which can be directly compared to the observed hadron spectra under the assumption of local parton hadron duality (LPHD) [13]. The ξ distribution is expected to be approximately Gaussian-shaped with the peak shifted to lower values for more massive particles. Such a shape has been seen at lower centre of mass energies [14]. Measurements of inclusive charged particles (predominantly charged pions) at the Z^0 pole [5, 15, 16] are described well by such a distribution with maxima at about 3.65. Identified mesons at the Z^0 peak show a shift of the maximum to lower values for heavier mesons. Peak values (ξ_{max}) of 4.11 ± 0.18 (π^0) [16], 2.62 to 2.91 for K^0 [5, 17] and 2.60 ± 0.15 for the η [18] have been reported.

Figure 4b shows the ξ distributions for Λ and Ξ^- together with the previously published K^0 distribution from OPAL [17]. The Λ and Ξ^- distributions show only a small shift of the maximum with respect to the K^0. We find a position of the maximum using a Gaussian fit for Λ's of $\xi^{\Lambda}_{max} = 2.77 \pm 0.05$, in good agreement with 2.82 ± 0.25 from [5]. For the Ξ^- we measure $\xi^{\Xi^-}_{max} = 2.57 \pm 0.11$.

After integrating the measured differential cross section for Λ and Ξ^- and adding the fractions predicted by Jetset for the unobserved momentum ranges, a correction of $3.7 \pm 1.8\%$ and $10 \pm 5\%$ respectively, the following total yields per hadronic Z^0 decay are obtained:

- $\Lambda,\bar{\Lambda}$/event $= 0.351 \pm 0.003$ (stat) ± 0.019 (syst)
- $\Xi^-,\bar{\Xi}^+$/event $= 0.0206 \pm 0.0011$ (stat) ± 0.0019(syst)

If method 2 for the Λ selection is used, we obtain a Λ yield per event in agreement with the above number to within 2%.

To obtain the yields for the decuplet baryons, the integrated efficiency is used, because the differential momentum spectrum is still dominated by large statistical errors. The systematic errors introduced by this procedure are estimated to be smaller than 5% and are included in the errors given below. We obtain the following numbers:

- $\Sigma(1385)^{\pm}, \bar{\Sigma}(1385)^{\pm}$/event $= 0.0380 \pm 0.0038$(stat) ± 0.0049 (syst)

- $\Xi(1530)^0, \bar{\Xi}(1530)^0$/event = 0.0063 $\pm$ 0.0010(stat) $\pm$ 0.0010 (syst)
- $\Omega^-, \bar{\Omega}^+$/event = 0.0050 $\pm$ 0.0012(stat) $\pm$ 0.0009 (syst)

These numbers are summarized in table 5. Using the above measurements, the following ratios are found:

- $\Xi^-/\Lambda = 0.0587 \pm 0.0069$
- $\Xi(1530)^0/\Sigma(1385)^{\pm} = 0.166 \pm 0.046$
- $\Omega^-/\Xi(1530)^0 = 0.79 \pm 0.30$

where the errors include both the statistical and systematic contributions and correlated errors have been neglected.

5 Comparison with the Lund Diquark Model

To test baryon production models via diquarks, we use the Jetset Monte Carlo. Within this diquark scheme, several parameters are relevant to baryon production:

- the diquark to quark ratio (qq/q),
- the strange to non-strange quark ratio (s/d),
- the strange diquark suppression factor (us/ud)$\times$(d/s),
- the spin 1 diquark parameter $\frac{1}{3}(qq_1/qq_0)$, and
- the popcorn parameter.

The diquark to quark ratio regulates the overall baryon rate and the s/d suppression is mainly determined by the kaon yield. In Jetset, Λ's are produced to a large extent from the combination of ud-diquarks and a single s quark. Thus, the single s quark contributes to the Λ and K^0 yield in about the same way and the ratio of the two particle yields is almost proportional to the ratio of ud-diquark to d-quarks in the fragmentation process. An uncertainty of about 20% exists, however, because Λ's are also produced via strange diquarks and from the decays of decuplet baryons. Table 5 shows the baryon yields obtained using Jetset with its default parameters, qq/q = 0.1, s/d=0.3, (us/ud)$\times$(d/s)=0.4, $\frac{1}{3}(qq_1/qq_0)$=0.05 and 50% popcorn probability. The strange octet baryons are described to within 20%. A simple change of the (us/ud)$\times$(d/s) parameter to 0.3$\pm$0.03 results in a good description of the K^0, Λ, and Ξ^- rates, as shown in table 5 ("Jetset tuned"). However, the decuplet baryons are, in general, not well described. The corresponding baryon rates from the Herwig Monte Carlo version 5.0 [6] with its default parameters are also shown in table 5. Even after changing the

cluster mass parameter from its default value of 3.5[6] to 3.32 ± 0.05 ("Herwig tuned"), the other baryons differ by up to a factor of three from the measured values, although the Ω^- rate is described.

To investigate whether the different decuplet baryon rates can be reproduced by Jetset, we have performed further studies. In these studies the parameter s/d was fixed to 0.285 to describe our measured K^0 yield [17]. The parameter qq/q was left unchanged from its default value of 0.1 since it describes the measured K^0 and Λ yields. The other three parameters, which mainly determine the relative baryon production rates, were varied over a wide range. No clear evidence for or against the popcorn mechanism exists: we accordingly used values of 0%, 50% and 100% for the popcorn parameter.

The popcorn parameter [19] defines the probability to form an additional meson between a baryon-antibaryon pair. Two additional parameters exist within the popcorn scheme as implemented in Jetset. These additional parameters regulate the strangeness suppression if a meson is produced between the baryon-antibaryon pair. Their default values result in additional suppression of strange mesons and baryons. Because of simple spin counting, the production of decuplet baryons relative to octet baryons is enhanced, if mesons are produced between the baryon and the antibaryon. No additional parameters are implemented, which would modify this decuplet enhancement.

To simplify the comparison of the results for the strangeness and spin suppression diquark parameters, we modified the popcorn model to have identical strange quark treatment for the different popcorn values. To do so, the two additional parameters within the popcorn scheme were changed from the default value of 0.5 to 1. Table 6 gives a summary of the results. The parameters (us/ud) × (d/s) and $\frac{1}{3}(qq_1/qq_0)$ were varied to give agreement with the octet baryons and either the $\Sigma(1385)^{\pm}$ (column 1 of each popcorn value) or the $\Xi(1530)^0$ (column 2 of each popcorn value) yield. We were not able to describe the Ω^- yield by this approach.

From these studies, we find that the diquark parameters are strongly correlated and can only be estimated accurately if the popcorn parameter is first fixed. We also find that the ratios of the inclusive yields for Ξ^-/Λ and $\Xi(1530)^0/\Sigma(1385)^{\pm}$ or $\Omega^-/\Xi(1530)^0$ cannot be varied independently within the current model. For all studied parameters, the ratio values obtained from the Monte Carlo are shown by the hatched bands in figures 5a and 5b and are in disagreement with the measurements.

For a more sophisticated and conclusive study of diquark models, more measurements of other baryon species and also of correlations are clearly needed.

6 Summary

We have measured the production cross sections of several strange octet and decuplet baryons in hadronic Z^0 decays.

[6]The default value in version 5.4 has been changed to 3.35 to describe the measured OPAL Λ rate.

From our measurements, the following conclusions on baryon production models can be drawn:

- the momentum spectrum of the Λ is softer than the one which is predicted by either the Jetset or the Herwig Monte Carlo,
- the default values for baryon production within the Jetset diquark scheme need only small modifications to describe the octet baryon yields, if the decuplet results are ignored,
- the Herwig Monte Carlo, with fewer free parameters, cannot describe the overall observed octet or decuplet baryon rates,
- the yields of the different decuplet baryons cannot be described by just one spin 1 suppression factor, and
- the amount of diquark splitting due to the popcorn mechanism has a strong influence on the other parameter values and no accurate determination of the various diquark parameters is possible without a better knowledge of the importance of the popcorn mechanism.

Acknowledgements

We thank T. Sjöstrand for various interesting discussions about section 5 of this letter.
We also thank the SL Division for the efficient operation of the LEP accelerator and their continuing close cooperation with our experimental group. In addition to the support staff at our own institutions we are pleased to acknowledge the
Department of Energy, USA,
National Science Foundation, USA,
Science and Engineering Research Council, UK,
Natural Sciences and Engineering Research Council, Canada,
Israeli Ministry of Science,
Minerva Gesellschaft,
Japanese Ministry of Education, Science and Culture (the Monbusho) and a grant under the Monbusho International Science Research Program,
American Israeli Bi-national Science Foundation,
Direction des Sciences de la Matière du Commissariat à l'Energie Atomique, France,
Bundesministerium für Forschung und Technologie, FRG,
National Research Council of Canada, Canada,
A.P. Sloan Foundation and Junta Nacional de Investigação Científica e Tecnológica, Portugal.

References

[1] See for example: D. Saxon, RAL-88-102;
P. Mättig, Phys. Rep. **177** (1989) 141.

[2] Particle Data Group, K. Hikasa *et al.*, Phys. Rev **D45** (1992) 1.

[3] See [1] and also MARK2 Collab., S.R. Klein *et al.*, Phys. Rev. Lett. **59** (1987) 2412.

[4] B. Anderson et al., Phys. Rep. **97** (1983) 31;
T. Sjöstrand, Comp. Phys. Comm. **39** (1986) 347 and CERN-TH.6488/92;
T. Sjöstrand and M. Bengtsson, Comp. Phys. Comm. **43** (1987) 367

[5] DELPHI Collab., P. Abreu *et al.*, Phys. Lett. **B275** (1992) 231.

[6] G. Marchesini *et al.*, Cambridge preprint Cavendish-HEP-91/26 and DESY 91-048.

[7] OPAL Collab., M. Ahmet *et al.*, Nucl. Instrum. and Meth. **A305** (1991) 275.

[8] M. Hauschild *et al.*, Nucl. Instrum. and Meth. **A314** (1992) 74.

[9] P. Billoir, Nucl. Instrum. and Meth. **225** (1984) 352.

[10] OPAL Collaboration, G. Alexander *et al.*, Z. Phys. **C52** (1991) 175.

[11] J. Allison *et al.*, CERN-PPE/91-234, submitted to Nucl. Instrum. and Meth.

[12] Y.I. Azimov, Y.L. Dokshitzer, V.A. Khoze and S.I. Troyan, Z. Phys. **C27** (1985) 65;
Y.L. Dokshitzer, V.A. Khoze and S.I. Troyan, *Perturbative QCD*, ed. A.H. Mueller,
Singapore: World Scientific 1989;
V.A. Khoze, Y.L. Dokshitzer and S.I. Troyan, LUND Preprint LU TP 90-12 (1990).

[13] D. Amati and G. Veneziano, Phys. Lett. **B83** (1979) 87;
Y.I.Azimov, Y.L.Dokshitzer, V.A.Khoze and S.I.Troyan, Phys. Lett. **B165** (1985).

[14] TASSO Collab., M. Althoff *et al.*, Z. Phys. **C22** (1984) 307.

[15] OPAL Collab., M. Z. Akrawy *et al.*, Phys. Lett. **B247** (1990) 617.

[16] L3 Collab., B. Adeva *et al.*, Phys. Lett. **B259** (1991) 119.

[17] OPAL Collab., G. Alexander *et al.*, Phys. Lett. **B264** (1991) 219.

[18] L3 Collab., O. Adriani *et al.*, CERN-PPE/92-83.

[19] B. Andersson, G. Gustafson and T. Sjöstrand, Physica Scripta **32** (1985) 574.

[20] OPAL Collab., P.D. Acton *et al.*, Z. Phys. **C53** (1992) 539.

Table Captions

Table 1: Number of observed baryon species and the different systematic errors of the measurements.

Table 2: Differential cross sections for Λ particles (symbols are defined in the text).

Table 3: Differential cross sections for Ξ^- particles (symbols are defined in the text).

Table 4: Differential cross sections $\Sigma(1385)^{\pm}$ and $\Xi(1530)^0$ particles (symbols are defined in the text).

Table 5: Inclusive particle yields as measured by OPAL (the statistical and systematic errors are added in quadrature). The values for $n_{charged}$ and K^0 are taken from [20] and [17]. The predictions are from the Jetset and Herwig Monte Carlo programs with default parameters. To describe the octet baryons the extra strangeness suppression value for diquarks in Jetset has been changed to 0.3 from the default of 0.4. For the Herwig Model the cluster mass parameter has been changed to 3.32 to describe the Λ yield.

Table 6: A comparison of inclusive yields with the Jetset Monte Carlo tuned to get agreement with K^0, Λ, Ξ^- and with either the $\Sigma^{\pm}(1385)$ (first column for each popcorn value) or the $\Xi^0(1530)$ measurement (second column). The measured and tuned decuplet numbers are bold faced. The parameters used are defined in the text.

Figure Captions

Figure 1a: Invariant mass $p\pi^-$, method 1.

Figure 1b: Invariant mass $p\pi^-$, method 2.

Figure 1c: Λ efficiency as a function of the scaled momentum, full line method 1, dashed line method 2, for the decay $\Lambda \rightarrow p\pi^-$.

Figure 2a: Invariant mass distribution for $\Lambda\pi^-$. The histogram shows the wrong charge combination $\Lambda\pi^+$.

Figure 2b: Ξ^- efficiency as a function of the scaled momentum for the decay chain $\Xi \rightarrow \Lambda\pi^-$ and $\Lambda \rightarrow p\pi^-$.

Figure 3a: Invariant mass distribution for ΛK^-. The histogram shows the background from the wrong charge combination ΛK^+ and from the remaining Ξ^- events. The ΛK mass of the Ξ^- decays is also shown as the shaded histogram.

Figure 3b: Invariant mass distribution for $\Lambda\pi^\pm$. The curves show the result of the fit to the data. The lowest curve represents the Gaussian and Breit-Wigner functions, centered on the Ξ^- and $\Sigma(1385)^\pm$ masses, respectively.

Figure 3c: Invariant mass distribution for $\Xi^-\pi^+$. The histogram shows the distribution obtained using wrong charge combination Ξ^+ paired with π^-.

Figure 4a: Differential cross sections $(1/N_{had})dn/dx_E$ for Λ, $\Sigma(1385)^\pm$, Ξ^-, and $\Xi(1530)^0$. The curves show the respective Monte Carlo differential cross sections from Jetset. Very similar differential cross sections are obtained with the Herwig Monte Carlo program.

Figure 4b: The differential cross sections $(1/N_{had})dn/d\ln(1/x_p)$ for K^0, Λ and Ξ^-.

Figure 5a: The ratio of the decuplet baryons $\Xi(1530)^0/\Sigma(1385)^\pm$ versus the ratio of the octet baryons Ξ^-/Λ, both for data ($\star$) and the Jetset Monte Carlo ($\bullet$). The elipses show the 1 and 2 statistical and systematic sigma errors. The shaded area shows ratios obtained with parameter changes described in the text.

Figure 5b: The ratio of the decuplet baryons $\Omega^-/\Xi(1530)^0$ versus the ratio of the octet baryons Ξ^-/Λ, both for data ($\star$) and the Jetset Monte Carlo ($\bullet$). The elipses show the 1 and 2 statistical and systematic sigma errors. The shaded area shows ratios obtained with parameter changes described in the text.

source of error	$\Lambda_{Method1}$	$\Lambda_{Method2}$	Ξ^-	Ω^-	$\Sigma(1385)^{\pm}$	$\Xi(1530)^0$
signal events	17384	30041	726	47	2480	79
background events	7457	16016	388	42	28820	83
stat. error	0.9%	0.8%	5.3%	24%	10%	16%
background syst.	3%	5%	2%	7.3%	10%	5%
cut simulation	4%	4%	4%	5%	5%	5%
resolution	1.5%	4.5%	5%	5%	5%	5%
MC extrapolation	1.8%	1.8%	5%	5%	5%	5%
MC statistic	1%	1%	3.5%	13%	1.4%	13%
total systematic	5.6%	8%	9%	17%	13%	16%

Table 1:

x_E	$< x_E >$	n	efficiency	$(1/N_{had})dn/dx_E$	ξ	$(1/N_{had})dn/d(\xi)$
0.027-0.035	0.031	1092 ± 37	0.070±.002	6.14 ± 0.26	4.47-3.69	0.063 ± 0.003
0.035-0.04	0.037	1078 ± 37	0.129±.004	5.28 ± 0.23	3.69-3.45	0.112 ± 0.005
0.04-0.05	0.045	1901 ± 56	0.143±.003	4.20 ± 0.15	3.45-3.13	0.131 ± 0.005
0.05-0.06	0.055	1921 ± 63	0.205±.004	2.96 ± 0.11	3.13-2.90	0.129 ± 0.005
0.06-0.07	0.065	1555 ± 56	0.214±.004	2.30 ± 0.09	2.90-2.72	0.127 ± 0.005
0.07-0.08	0.075	1329 ± 46	0.220±.005	1.91 ± 0.08	2.72-2.58	0.129 ± 0.005
0.08-0.10	0.089	2164 ± 56	0.228±.004	1.50 ± 0.05	2.58-2.33	0.124 ± 0.004
0.10-0.15	0.122	2979 ± 68	0.211±.005	0.893 ± 0.029	2.33-1.91	0.105 ± 0.003
0.15-0.20	0.173	1536 ± 48	0.181±.006	0.535 ± 0.024	1.91-1.62	0.091 ± 0.004
0.20-0.30	0.244	1257 ± 44	0.143±.005	0.278 ± 0.014	1.62-1.21	0.068 ± 0.003
0.30-0.40	0.344	386 ± 25	0.089±.004	0.136 ± 0.011	1.21-0.92	0.047 ± 0.003
0.40-0.50	0.443	153 ± 16	0.073±.006	0.066 ± 0.009	0.92-0.69	0.0295 ± 0.004
0.50-0.60	0.543	33 ± 8.5	0.046±.006	0.023 ± 0.007	0.69-0.51	0.0127 ± 0.0036

Table 2:

x_E	$< x_E >$	n	efficiency	$(1/N_{had})dn/dx_E$	ξ	$(1/N_{had})dn/d(\xi)$
0.035-0.05	0.037	56 ± 10.9	0.047±.007	0.252 ± 0.060	3.91-3.19	0.0052 ± 0.0013
0.05 -0.10	0.073	313 ± 25.4	0.153±.008	0.129 ± 0.013	3.19-2.34	0.0076 ± 0.0008
0.10-0.15	0.122	174 ± 18.4	0.171±.012	0.064 ± 0.008	2.34-1.91	0.0074 ± 0.0009
0.15-0.20	0.173	78 ± 13.4	0.151±.015	0.033 ± 0.006	1.91-1.61	0.0055 ± 0.0010
0.20-0.25	0.222	45 ± 10.1	0.121±.016	0.024 ± 0.006	1.61-1.39	0.0055 ± 0.0014
0.25-0.30	0.273	33 ± 7.7	0.088±.016	0.024 ± 0.007	1.39-1.20	0.0063 ± 0.0018
0.30-0.50	0.372	25 ± 7.1	0.067±.011	0.0059 ± 0.002	1.20-0.69	0.0023 ± 0.0008

Table 3:

x_E	n($\Sigma(1385)^{\pm}$)	efficiency	$(1/N_{had})dn/dx_E$	n($\Xi(1530)^0$)	efficiency	$(1/N_{had})dn/dx_E$
0.05-0.1	1297±187	0.286	0.327 ±0.047	43±8.8	0.067	0.061±0.019
0.1 -0.2	617±142	0.316	0.070 ±0.016	19±7.9	0.092	0.0098±0.0046
0.2 -0.3	210±74	0.273	0.028 ±0.010	12±4.9	0.0861	0.0066±0.0034

Table 4:

particle	n/event (OPAL)	Jetset default	Jetset tuned	Herwig default	Herwig tuned
$n_{charged}$	21.4 ±0.43	21.3	21.3	20.9	21.1
K^0	2.10 ±0.14	2.16	2.15	2.07	2.12
Λ	0.351 ±0.019	0.383	0.351	0.427	0.352
Ξ^-	0.0206 ±0.0021	0.027	0.021	0.062	0.046
$\Sigma(1385)^{\pm}$	0.0380 ±0.0062	0.074	0.068	0.136	0.115
$\Xi(1530)^0$	0.0063 ±0.0014	0.0053	0.0048	0.0307	0.0216
Ω^-	0.0050 ±0.0015	0.00072	0.00044	0.0095	0.0054

Table 5:

	data	popcorn=0%		popcorn=50%		popcorn=100%	
us/ud×d/s		0.20	0.28	0.18	0.25	0.15	0.20
$\frac{1}{3} \times qq_1/qq_0$		0.04	0.15	0.012	0.08	0.008	0.05
K^0	2.10 ±0.14	2.11	2.11	2.12	2.11	2.11	2.10
Λ	0.351 ±0.019	.365	.356	.366	.353	.358	.342
Ξ^-	0.0206 ±0.0021	.0191	.0205	.0213	.0214	.0197	.0201
$\Sigma(1385)^{\pm}$	**0.0380 ±0.0062**	**.0374**	.0862	**.0382**	.0886	**.0385**	.0815
$\Xi(1530)^0$	**0.0063 ±0.0014**	.0019	**.0054**	.0027	**.0065**	.0026	**.0055**
Ω^-	0.0050 ±0.0015	.0001	.0006	.0003	.0009	.0003	.0006

Table 6:

Figure 1a

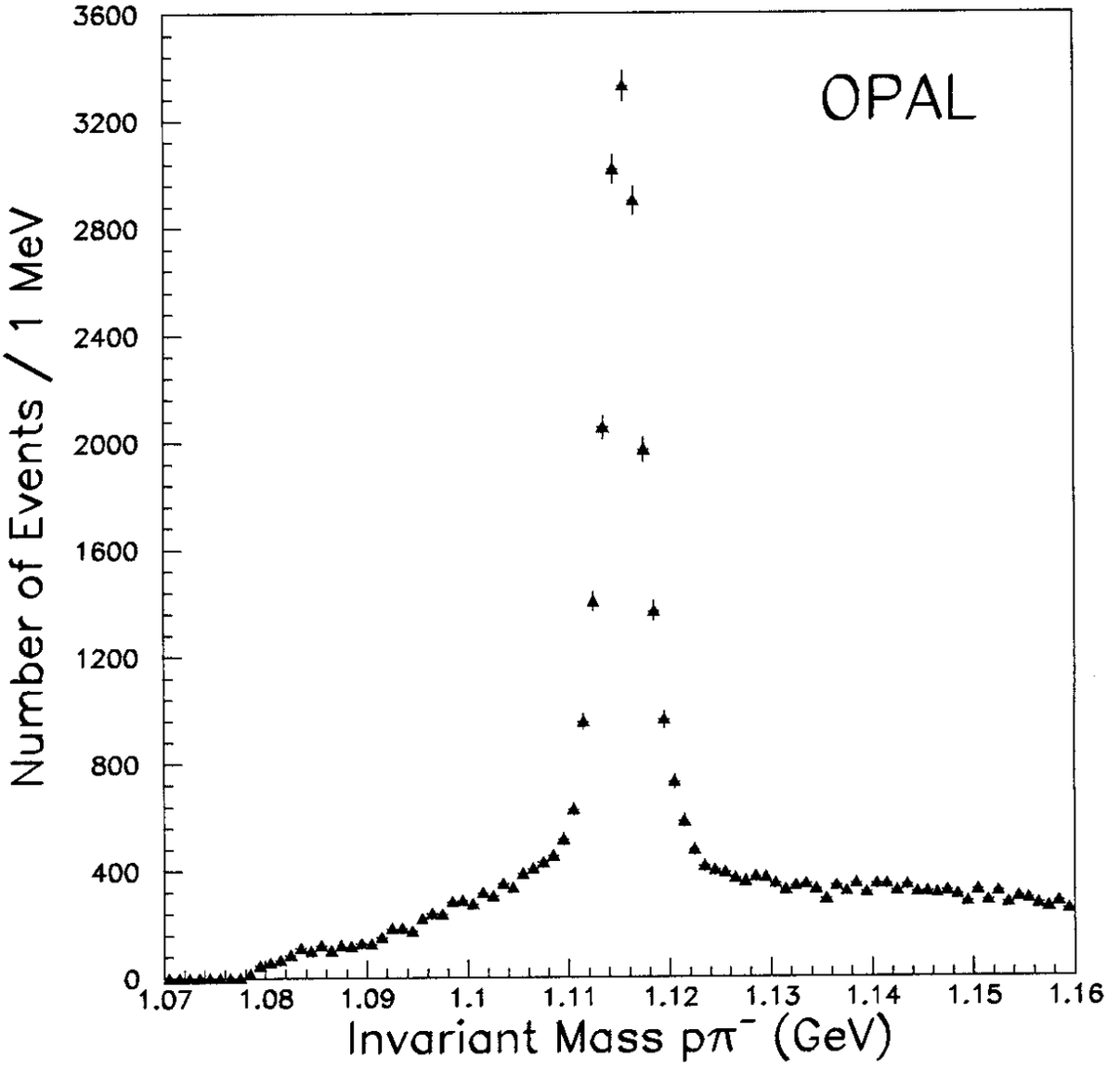
OPAL
Number of Events / 1 MeV
Invariant Mass pπ⁻ (GeV)
0
400
800
1200
1600
2000
2400
2800
3200
3600
1.07
1.08
1.09
1.1
1.11
1.12
1.13
1.14
1.15
1.16

Figure 1b

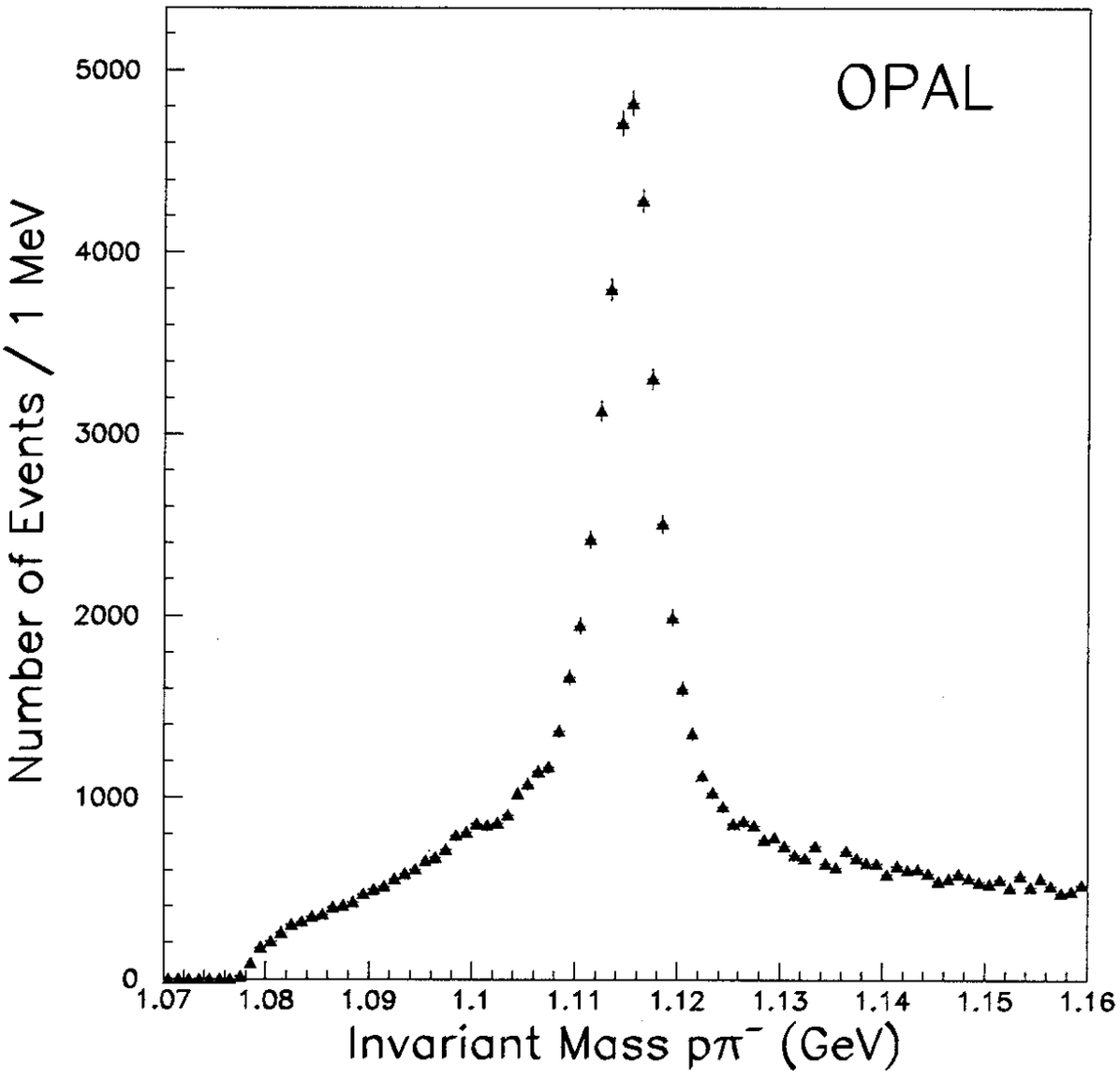
OPAL
Number of Events / 1 MeV
5000
4000
3000
2000
1000
0
1.07
1.08
1.09
1.1
1.11
1.12
1.13
1.14
1.15
1.16
Invariant Mass pπ⁻ (GeV)

Figure 1c

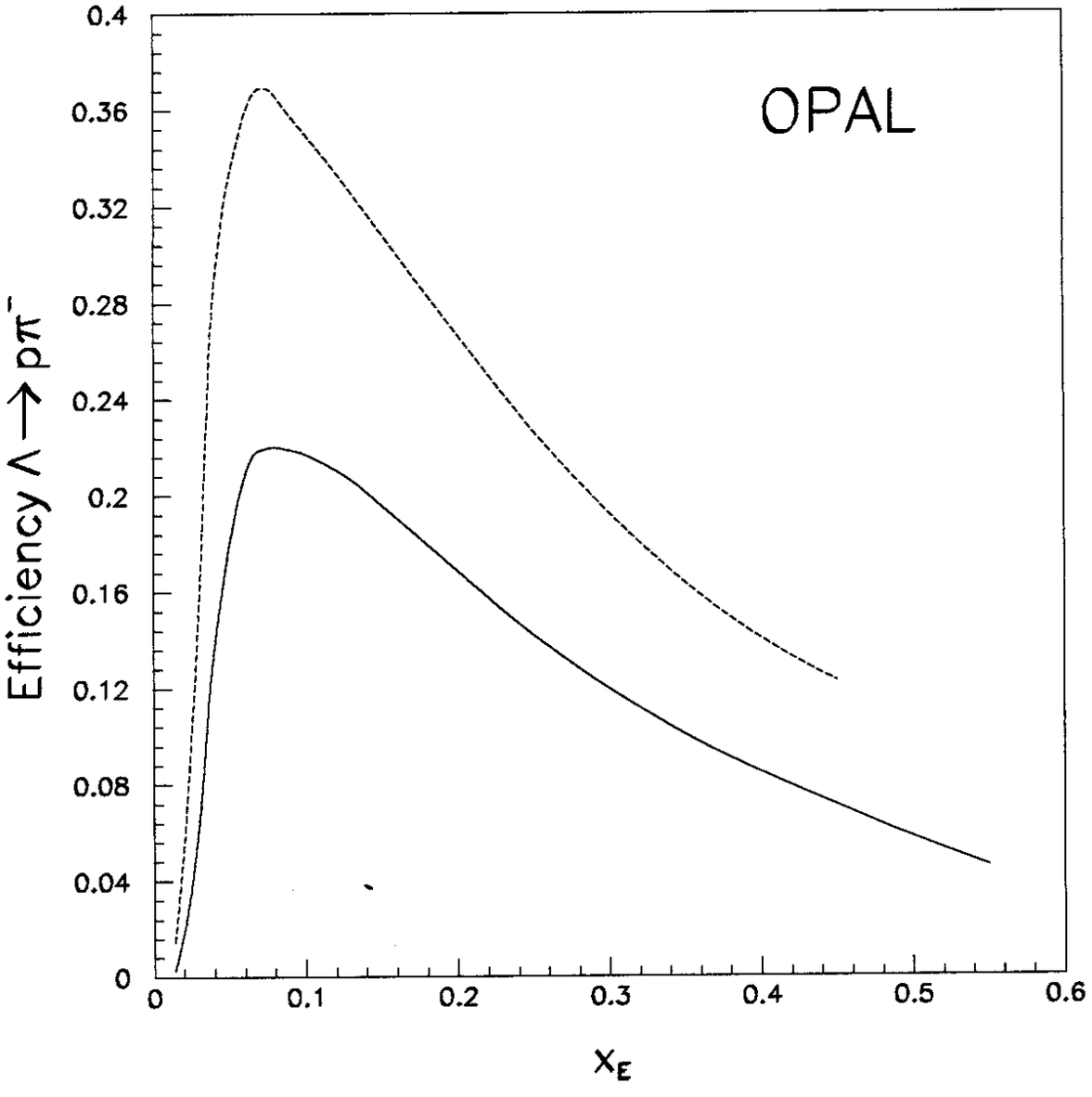
OPAL
Efficiency $\Lambda \rightarrow p\pi^-$
x_E
0.4
0.36
0.32
0.28
0.24
0.2
0.16
0.12
0.08
0.04
0
0
0.1
0.2
0.3
0.4
0.5
0.6

Figure 2a

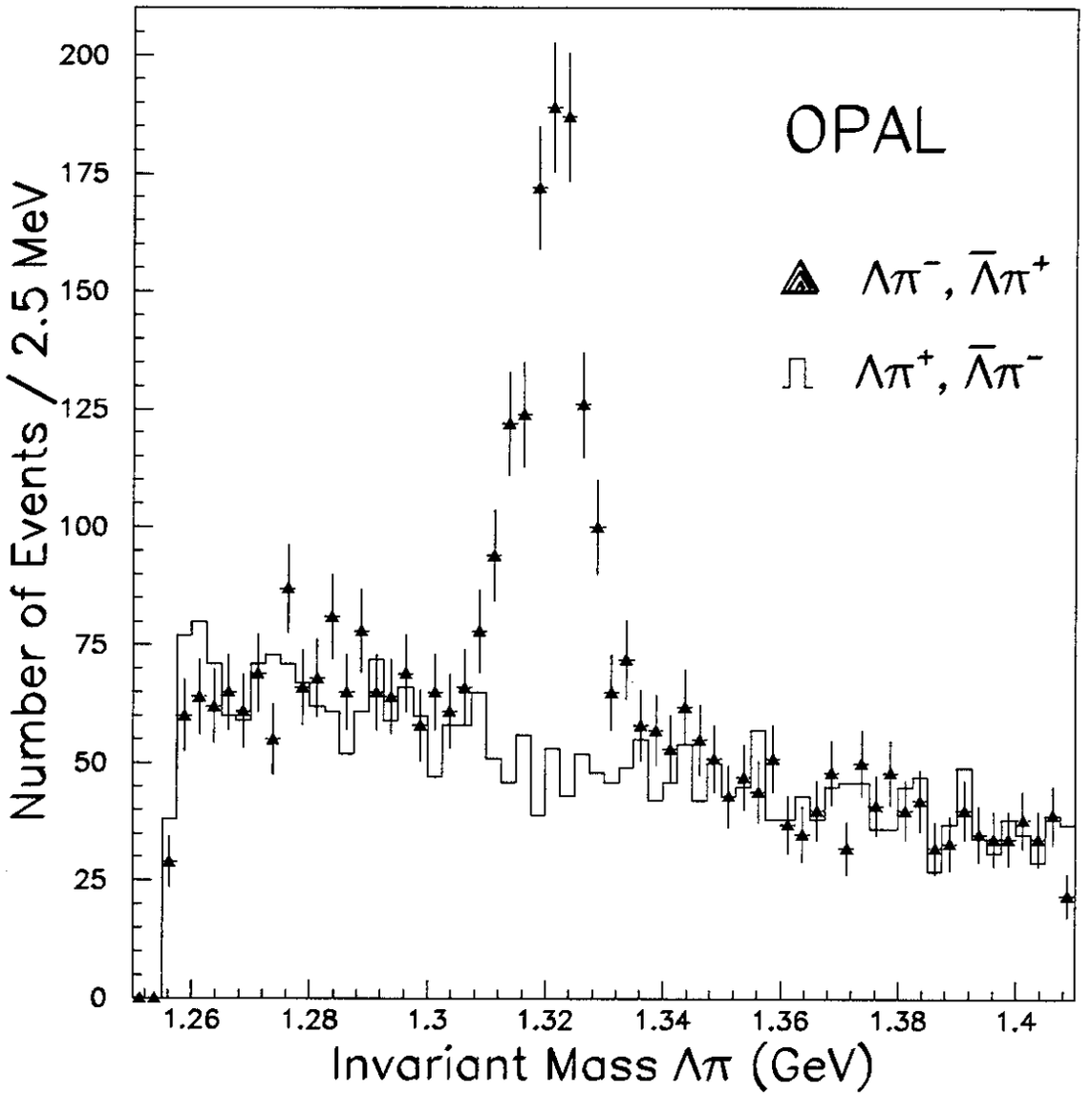
OPAL
$\Lambda\pi^-, \bar{\Lambda}\pi^+$
$\Lambda\pi^+, \bar{\Lambda}\pi^-$
Number of Events / 2.5 MeV
Invariant Mass $\Lambda\pi$ (GeV)
0
25
50
75
100
125
150
175
200
1.26
1.28
1.3
1.32
1.34
1.36
1.38
1.4

Figure 2b

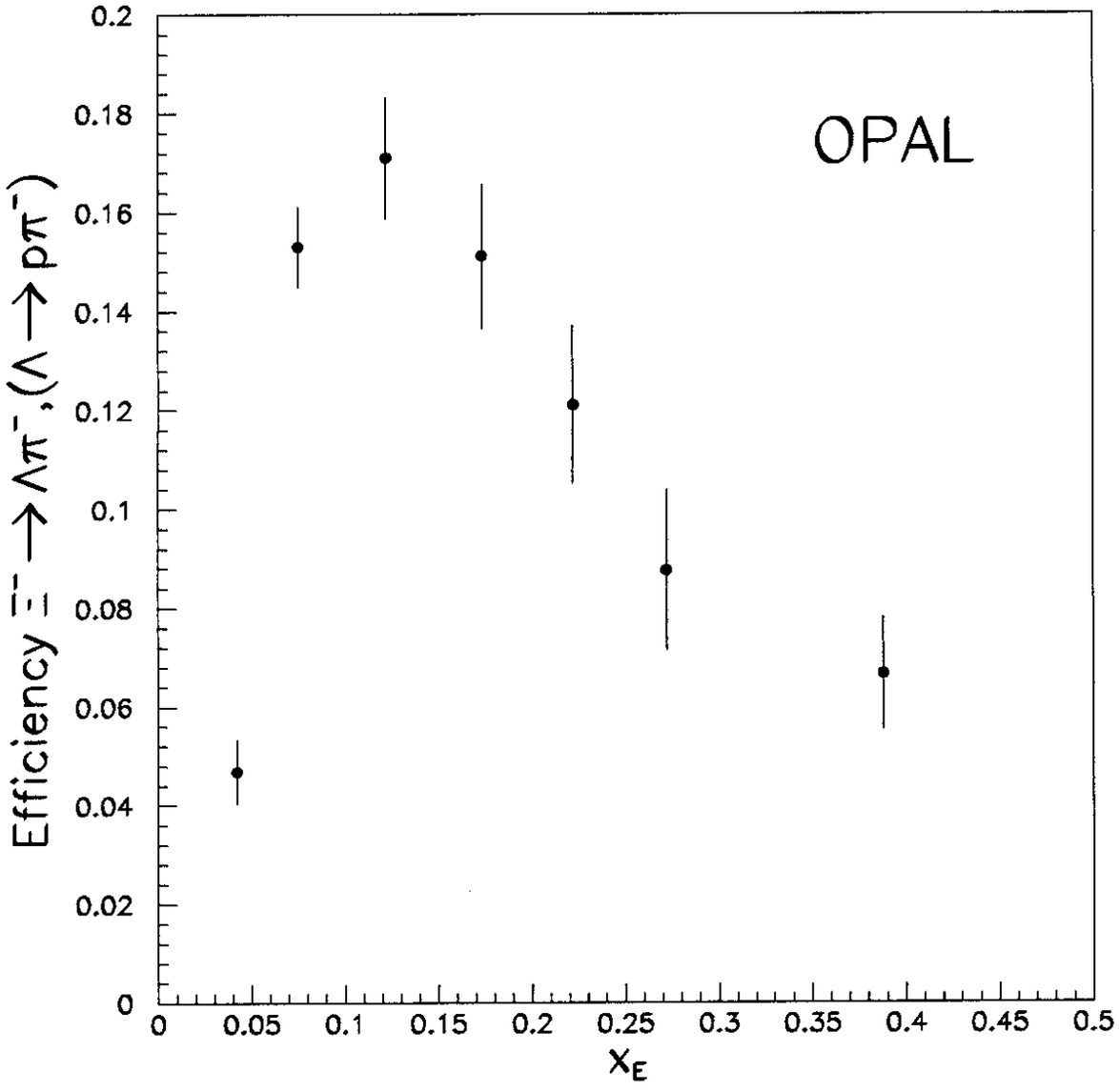
OPAL
Efficiency $\Xi^- \to \Lambda\pi^-, (\Lambda \to p\pi^-)$
x_E
0
0.02
0.04
0.06
0.08
0.1
0.12
0.14
0.16
0.18
0.2
0
0.05
0.1
0.15
0.2
0.25
0.3
0.35
0.4
0.45
0.5

Figure 3a

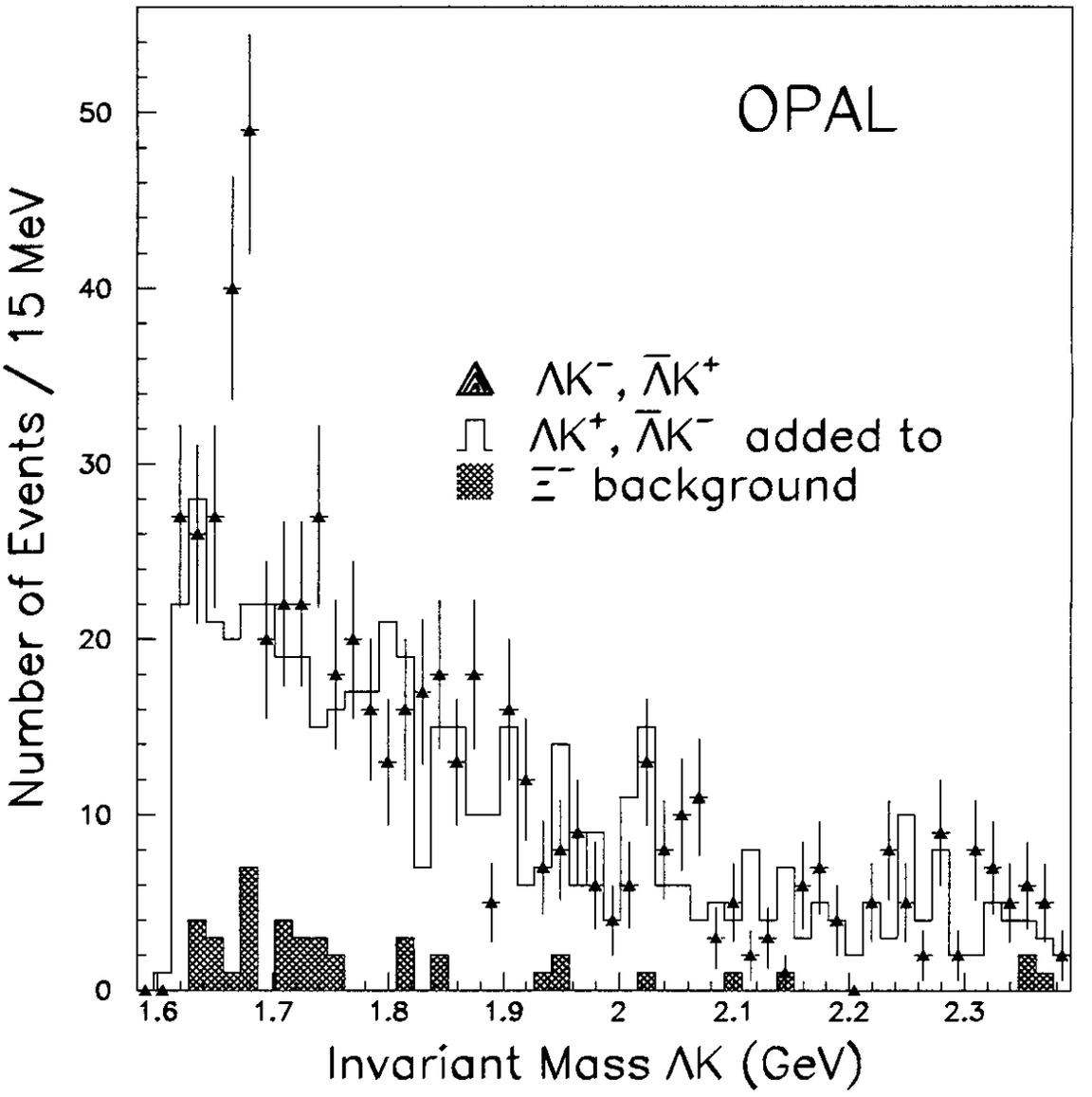
OPAL
$\Lambda K^-, \bar{\Lambda} K^+$
$\Lambda K^+, \bar{\Lambda} K^-$ added to
Ξ^- background
Number of Events / 15 MeV
Invariant Mass ΛK (GeV)
0
10
20
30
40
50
1.6
1.7
1.8
1.9
2
2.1
2.2
2.3

Figure 3b

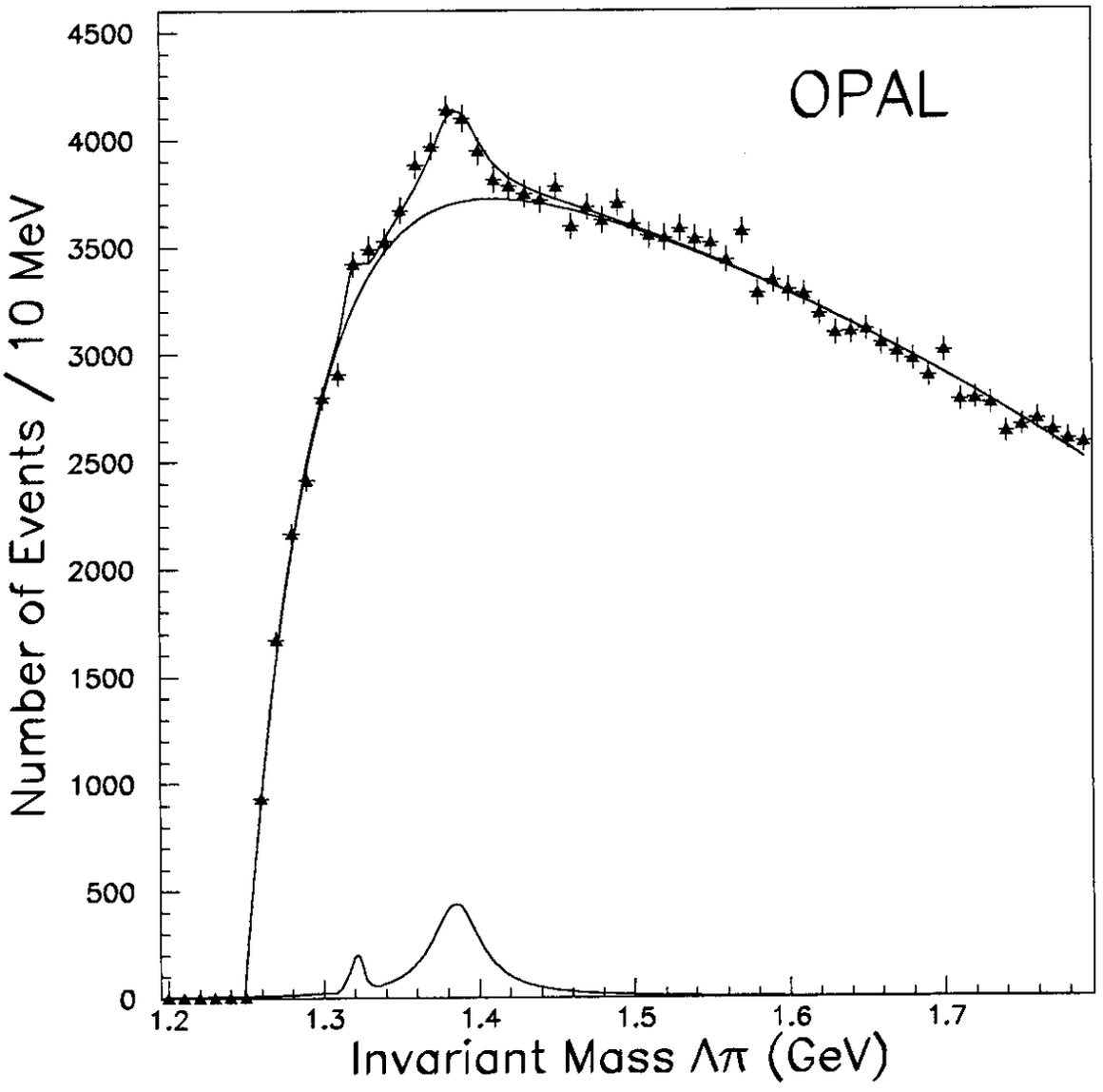
OPAL
Number of Events / 10 MeV
4500
4000
3500
3000
2500
2000
1500
1000
500
0
1.2
1.3
1.4
1.5
1.6
1.7
Invariant Mass Λπ (GeV)

Figure 3c

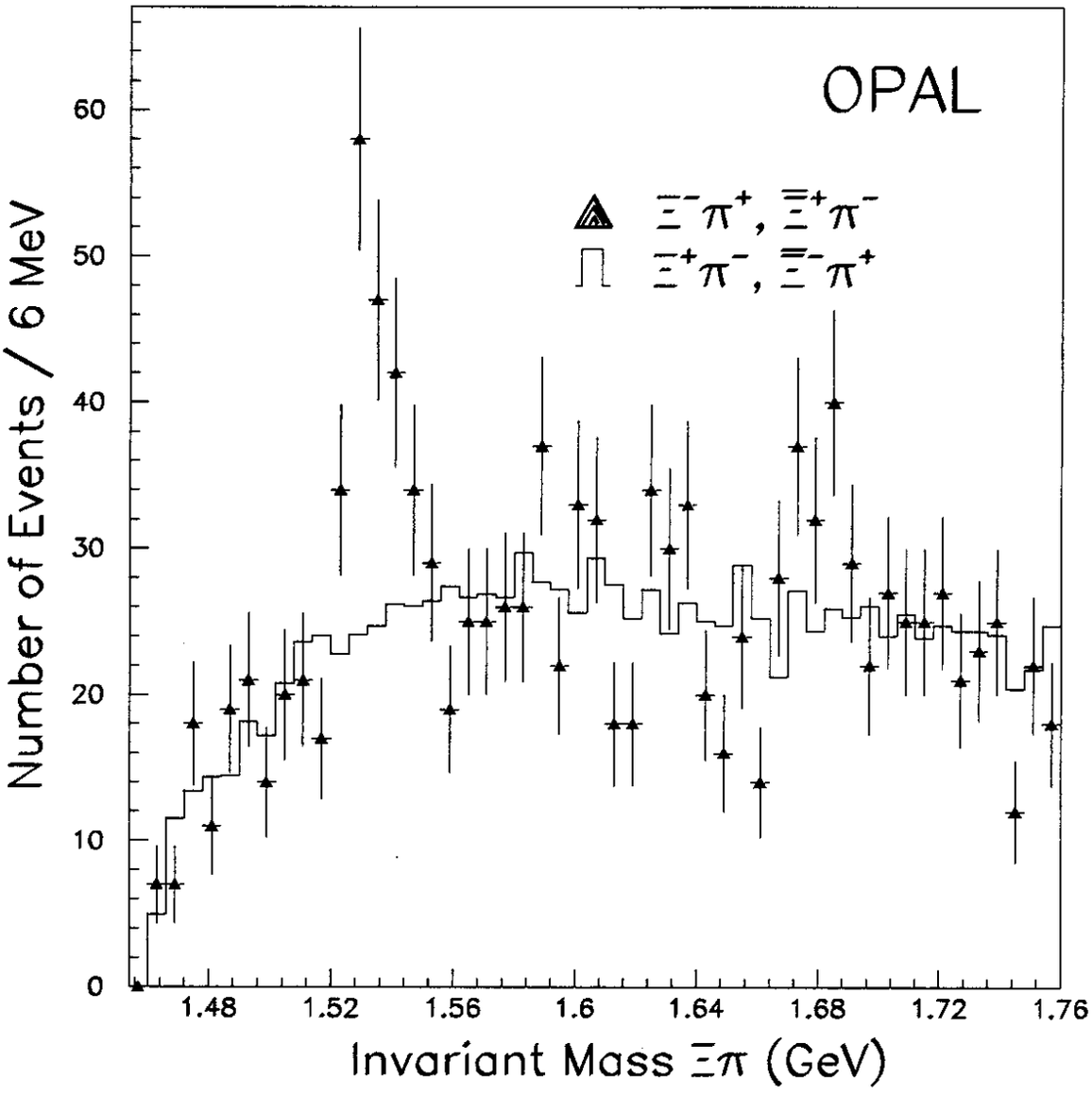
OPAL
$\Xi^-\pi^+$, $\bar{\Xi}^+\pi^-$
$\Xi^+\pi^-$, $\bar{\Xi}^-\pi^+$
Number of Events / 6 MeV
0
10
20
30
40
50
60
1.48
1.52
1.56
1.6
1.64
1.68
1.72
1.76
Invariant Mass $\Xi\pi$ (GeV)

Figure 4a

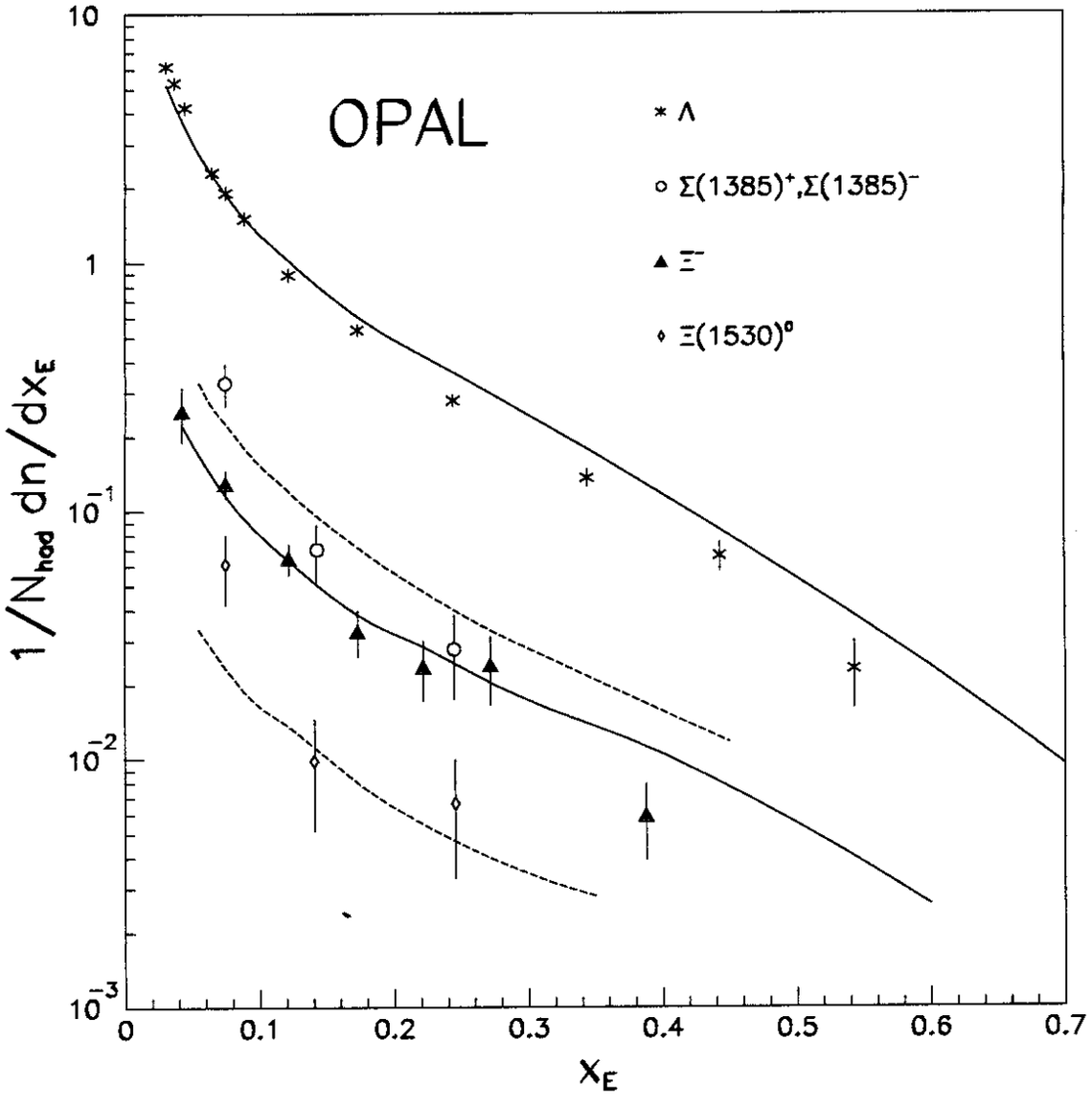
OPAL
* Λ
○ Σ(1385)⁺,Σ(1385)⁻
▲ Ξ⁻
◇ Ξ(1530)⁰
1/N_had dn/dx_E
x_E
10
1
10⁻¹
10⁻²
10⁻³
0
0.1
0.2
0.3
0.4
0.5
0.6
0.7

Figure 4b

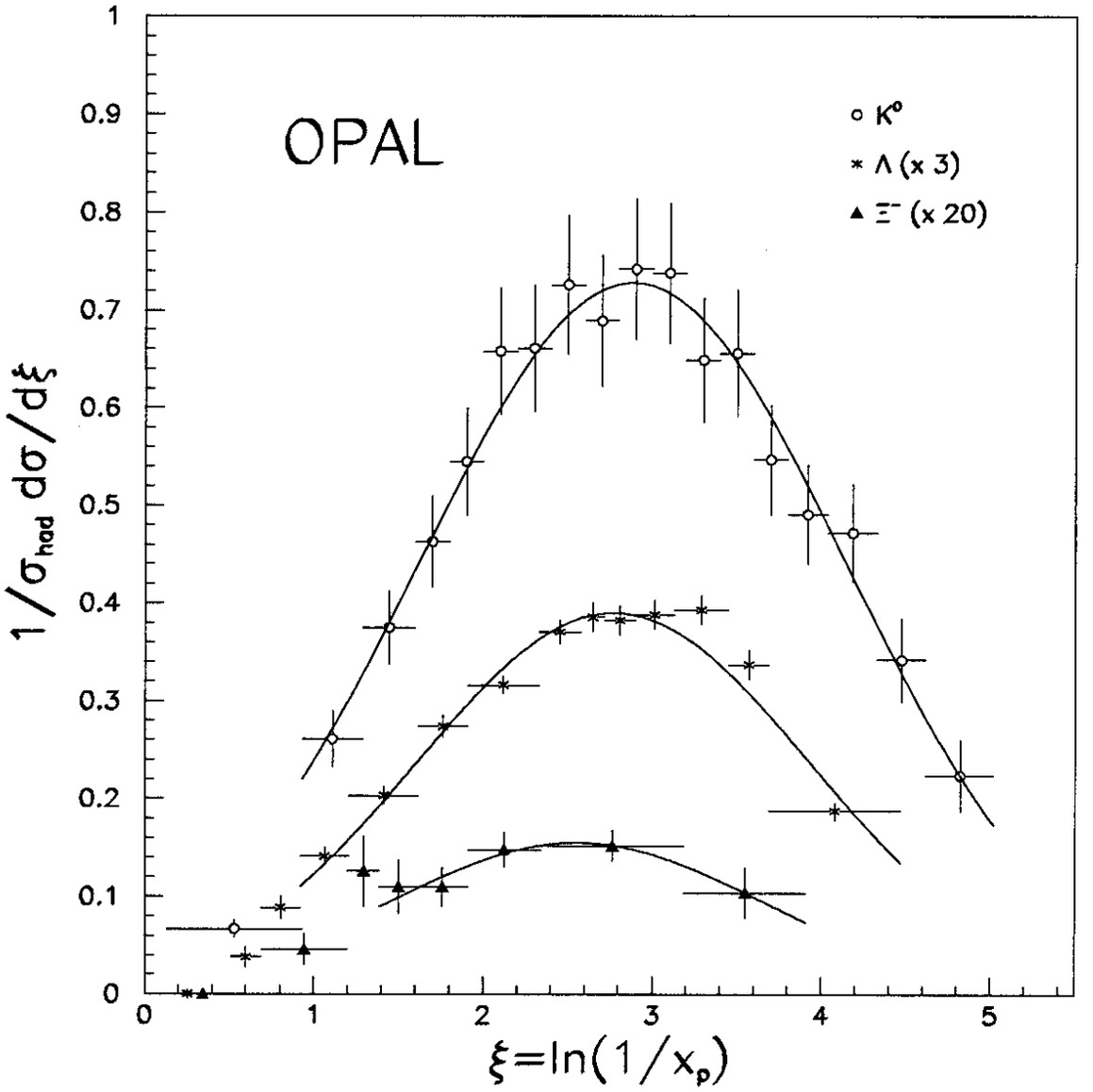
OPAL
K°
Λ (x 3)
Ξ⁻ (x 20)
1/σ_had dσ/dξ
ξ=ln(1/x_p)
0
0.1
0.2
0.3
0.4
0.5
0.6
0.7
0.8
0.9
1
0
1
2
3
4
5

Figure 5a

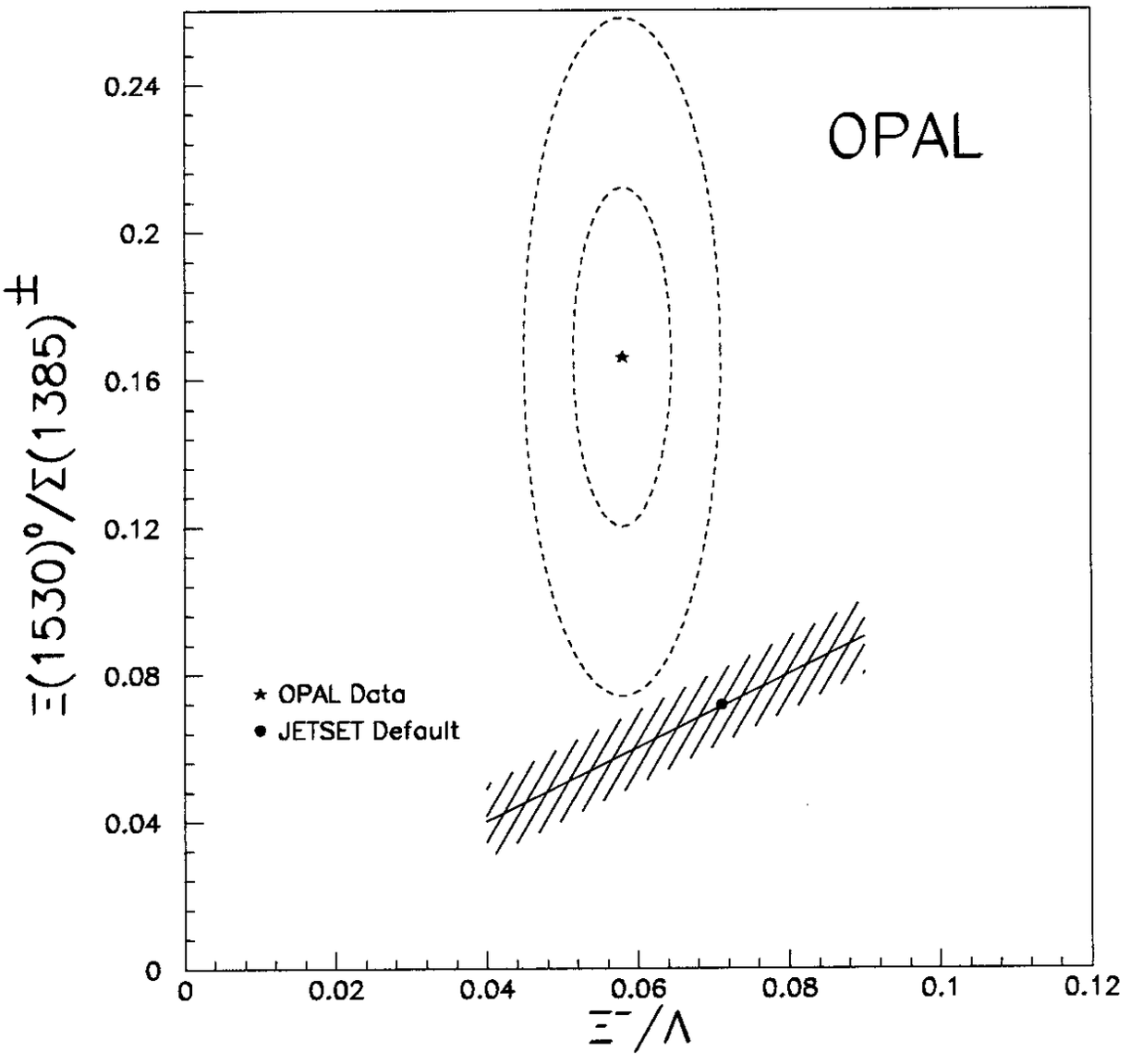
OPAL
0.24
0.2
0.16
0.12
0.08
0.04
0
0
0.02
0.04
0.06
0.08
0.1
0.12
Ξ(1530)°/Σ(1385)±
Ξ⁻/Λ
★ OPAL Data
● JETSET Default

Figure 5b

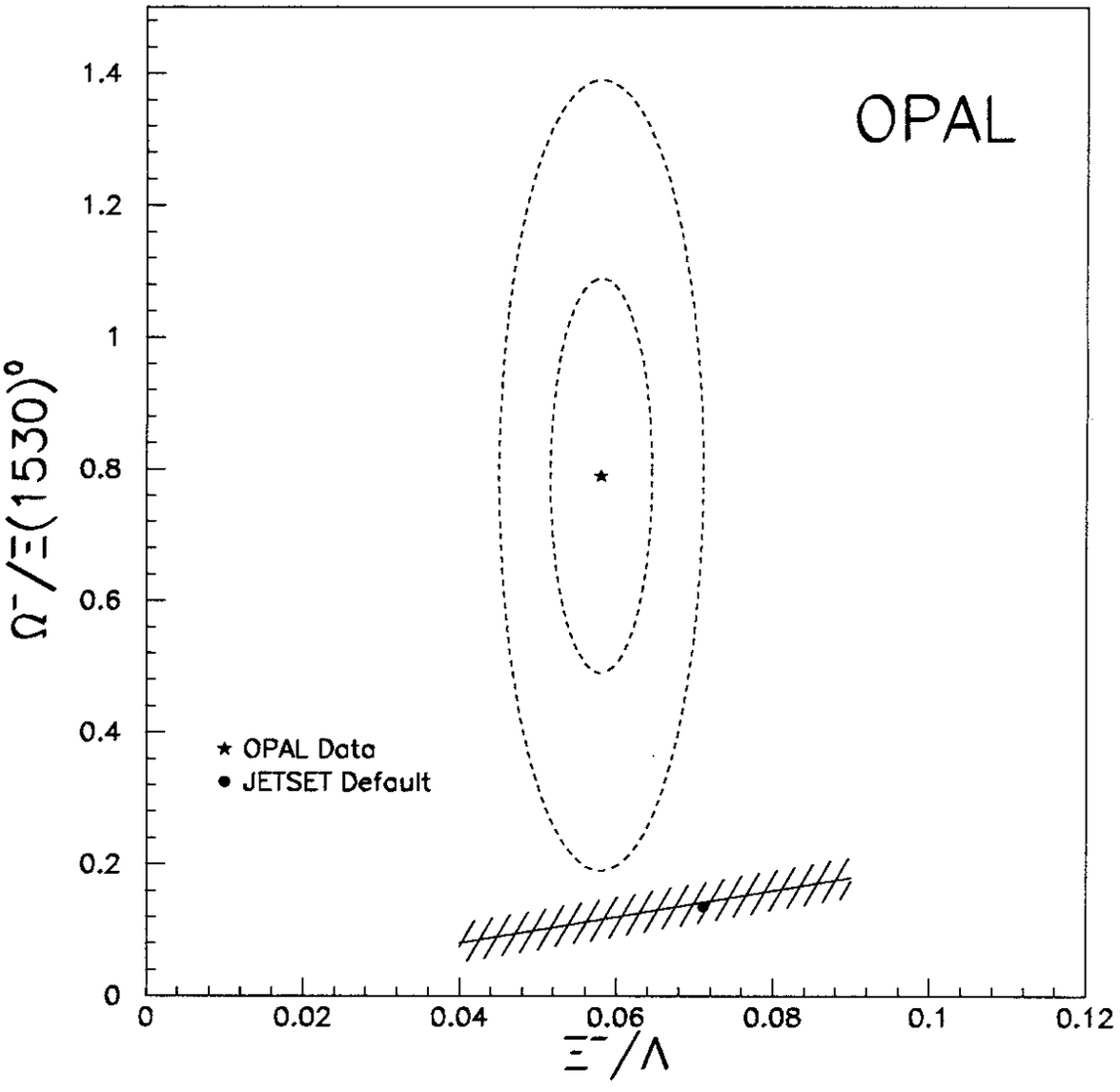
OPAL
★ OPAL Data
● JETSET Default
$\Omega^-/\Xi(1530)^0$
Ξ^-/Λ
0
0.2
0.4
0.6
0.8
1
1.2
1.4
0.02
0.04
0.06
0.08
0.1
0.12